PEDOT:PSS-based micromuscles and microsensors fully integrated in flexible chips

Kätlin Rohtlaid, Lauréline Seurre, Giao T M Nguyen, Garrett Curley, Caroline Soyer, Sébastien Grondel, Frederic Vidal, Cedric Plesse, Eric Cattan

IOP Publishing Smart Materials and Structures
Smart Mater. Struct.2 **XX** (XXXX) XXXXXX https://doi.org/XXXX/XXXX

PEDOT:PSS-Based Micromuscles and Microsensors Fully Integrated in Flexible Chips

Kätlin Rohtlaid[1], Lauréline Seurre[2], Giao T. M. Nguyen[1], Garrett Curley[2], Caroline Soyer[2], Sébastien Grondel[2], Frédéric Vidal[1], Cédric Plesse[1] and Eric Cattan[2]

[1] LPPI, EA2528, Institut des Matériaux, Université de Cergy-Pontoise, 5 mail Gay Lussac, Neuville sur Oise, F-95031 Cergy Cedex, France.
[2] Univ. Polytechnique des Hauts de France, CNRS, Univ. Lille, Yncrea, Centrale Lille, UMR 8520 - IEMN, DOAE, F-59313 Valenciennes, France

E-mail: eric.cattan@uphf.fr

Received xxxxxx
Accepted for publication xxxxxx
Published xxxxxx

Abstract

The demand for polymer-based soft micro-electro-mechanical systems (MEMS) is growing due to the substantial increase of flexible and wearable electronic devices. In this context, electronically conducting polymers (ECPs) fulfil the requirements for soft MEMS by offering the possibility of actuation and sensing, however, their miniaturization, their integration attempts and their resulting performances are still limiting their use in real applications. In this work, elaboration, integration and operation of soft and efficient microtransducers (MTs) based on commercially available poly(3,4-ethyledioxythiophene):poly(styrene sulfonate) (PEDOT:PSS) conductive ink into flexible chips is demonstrated. This original process overcomes existing hurdles to the fabrication of fully integrated ECP-based devices with gold remote contacts directly in contact with ECPs and further embedding in flexible support. These batch-fabricated chips are actuated at low voltage (±3.0 V) in open-air with individual accessible electrical connections. More importantly, the mechanical strain sensing is evidenced for the first time on such small ECP-based devices after full integration and demonstrating low impact of the microfabrication process. This work opens the way for further development of soft ECP-MEMS and integration into more complex systems with possible applications in microrobotics, microfluidics, optoelectronics, biology, medicine or space.

Keywords: electronically conducting polymers, sensing, microtransducers, micro-integration, flexible chips

1. Introduction

Classical MEMS based on stiff materials such as silicon, ceramic and metals face a hurdle when moving toward soft electronics. The development of polymer based soft MEMS compatible with soft substrates and tissues appears as a challenge for the next generation of electronics. Electronically conducting polymers (ECPs) are smart and soft materials that have been successfully used for the development of actuators for few decades now. They share interesting features with other electroactive polymer technologies such as being lightweight, silent, flexible and easy to process futhermore require only few volts to operate, which is a significant advantage at microscale or for integration with biological tissues. Their working principle is based on redox process, where during reversible oxidation-reduction reaction electrons are extracted or inserted along the polymer backbone, which is causing ions exchange and finally leading to dimensional

changes (expansion/contraction) of the ECPs.[1] The first ECP based microactuators date back to 1993, when Smela *et al.* fabricated millimeter-scale polymer fingers, made of polypyrrole (PPy) gold (Au) bilayer strips and operating in liquid electrolyte.[2] In the following years, a lot of progress was achieved by improving the materials and different designs to develop advanced microactuators for different microstructures, such as microbox, microrobotic arm, microfluidic system and cell clinic, able to function in specific surroundings (salt solutions, blood plasma, urine and cell culture medium).[3–10] Although ECP based microsystems were fabricated, they were still limited to the operation in liquid environment, hindering to enlarge their possible application fields. Using trilayer actuator configuration, composed of two electroactive electrodes sandwiching an ion storage membrane, allows the operation of the actuators in open-air.[5,11] While it may seem a straightforward next step to combine trilayer actuators with previously used microfabrication steps, the fabrication of first air-operating microactuator was finally accomplished in 2009, i.e. 16 years later.[12] In this case, the microactuator was fabricated as a conventional macroscale actuator and miniaturization of the device was obtained using laser ablation, resulting in simplistic microactuators which were operated using macroscopic electrical connections. Since 2009 and the demonstration of first air-operating microactuator, many efforts have been made to improve the fabrication, development and performances of microfabricated integrated devices. Different methods and combination of methods, such as laser ablation, reactive ion etching (RIE), wet chemical etching, photolithography and spin-coating have been used with numerous ECPs and actuator configurations. Unfortunately, to date, no systems fulfill the requirements for ECP-based microsystems, since the previously described systems have been reported with manual handling steps, without individual integrated remote electrical contacts, or presenting low performances.[13–24] Our group recently reported an easy and efficient fabrication method of trilayer microactuators based on poly(3,4-ethylenedioxythiophene):poly(styrene sulfonate) (PEDOT:PSS) commercial conductive ink.[25] While these devices were simply micropatterned using laser ablation and manually interfaced with macroscopic electrical connections, their material precursors and synthesis steps have been carefully chosen with their future integration into flexible supports in mind.

The elaboration of fully integrated microtransducers (MTs) based on ECPs as well as their operation as microactuators and microsensors is still a challenge. For that reason, in this paper, an innovative microfabrication process is proposed, comprising the integration of top and bottom electrical remote contacts without any manual handling during the microfabrication and carefully minimizing MTs damage by considering all the affecting risks for chosen materials. The process ensures the fabrication of individually controllable self-standing beams, embedded into soft polymeric support and resulting in foldable chips. The strain difference and blocking force of these proof-of-concept prototypes, used as actuators, were characterized in open-air and at low electrical potential (±3.0 V). Furthermore, on such small and fully integrated microdevices, the mechanical strain sensing is evidenced, thus offering new possibilities in the near future for more complex microsystems with the duality of actuation and sensing i.e. proprioception.

2. Results and Discussions

The chosen strategy relies on two elements. First the air-operating MTs are elaborated on Si substrate according to a layer stacking approach, being compatible with microfabrication processes (figure 1(a)).[25] Briefly, bottom PEDOT:PSS modified electrode is obtained from a casting-evaporation-polymerization step of formulated PEDOT:PSS/poly(ethylene oxide) (PEO) precursors aqueous dispersion. The ionic conducting membrane, based on PEO and nitrile butadiene rubber (NBR), is elaborated on top of the electrode by spin-coating and polymerizing a solution containing the PEO network precursors and the linear NBR chains. The top electrode is then elaborated according to the same procedure as the first one on top of the bilayer. A final free-radical polymerization of PEO precursors allows the formation of PEO network within each layer but also at their interfaces to promote strong adhesion and mechanical stability of the trilayer actuator. As the second key element, a microfabrication process is developed (i) to be compatible with PEDOT:PSS as a chosen ECP, (ii) to provide both, MTs fabrication and integration of electrical contacts and (iii) to lead to the final and operating flexible microdevice. Considering the properties of the PEDOT:PSS, a careful choice of techniques had to be made in order to not damage the previously elaborated materials. For instance, the process considers the hygroscopicity of the PEDOT:PSS, which means that all the photoresist developers that contain water have been eliminated from the process, leaving negative SU-8 as the only usable photoresist after the fabrication step of MTs. Related to that problem, also wet etching techniques are not used due to the involvement of aggressive liquid chemicals and additionally, the temperature of each processing step was verified carefully not to damage the PEDOT:PSS-based MTs.

The full microfabrication process was developed using high resolution photomasks and starting with a backside alignment due to the opacity of the PEDOT:PSS. The main steps in the microfabrication process are described in figure 1(b)-(e), however more detailed description of the process is brought in Experimental Section. The chips were built on a 2-inch Si wafer, obtaining the top gold electrode, MT,

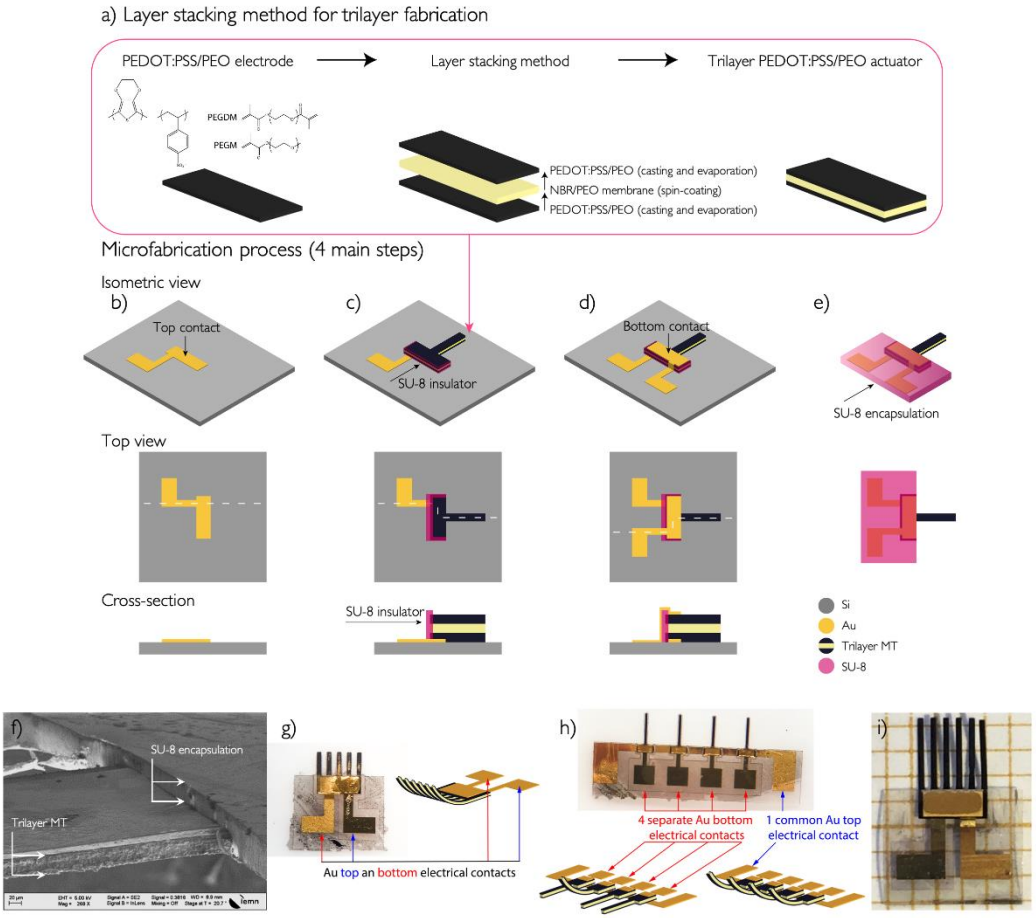

Figure 1. Schematic representation of the (a) layer stacking method; and microfabrication process in isometric, top and cross-sectional view: (b) Au top electrical contact, (c) patterned PEDOT:PSS-based MT and thin SU-8 insulator on the edge of the MT, (d)Au bottom electrical contact, (e) released chip with SU-8 encapsulation as the flexible support, (f) SEM image of the microbeam showing the edge of the MT after etching and the embedding in the SU-8 layer, (g) microcomb configuration of MT with integrated electrical remote contacts, (h) four microbeams with common top electrical contact and independent bottom electrical contacts, (i) characterized chip (2900 x 250 x 23 µm).

electrode and finally encapsulating partially the MT to obtain the flexible support. The top gold contacts (Ti (20 nm)/Au (300 nm) deposited by evaporation) were obtained using a standard lift-off process of photoresist S1828 to create the desired patterns directly on a wafer (figure 1(b)).The trilayer was fabricated according to the layer stacking method as described previously[25] and summarized above (figure 1(a)) and patterned using RIE to obtain MTs with desired shapes. In the next step, the gold bottom electrode has to start on silicon and finish 35µm higher on the top of the MT. To avoid short circuit between the PEDOT:PSS layers, we added a thin layer of SU-8 as an insulator, which covers the edge of the MT (figure 1(c) see arrow and the pink layer). Afterwards, Ti/Au were evaporated over the entire wafer and SU-8 photoresist was used to create local masks before ion beam etching (IBE), to obtain bottom electrical contacts (figure 1(d)). The next step included encapsulation of the electrical contacts and a part of MTs into SU-8 layer (the thickness is adjusted according to the desired stiffness of the chip) and finally by etching through the Si wafer to release the prototypes (figure 1(e)). The vertical wall of the MT after RIE and the embedding in the SU-8 layer are illustrated in the SEM image on figure 1(f). This batch microfabrication is obtained with only standardized processes that allows the design of different configurations of microactuators. Figure 1(g) presents a microcomb configuration where all the microbeams are connected with only one top and one bottom remote electrical contact and electrical stimulation leads to their simultaneous bending. Another chip configuration in figure 1(h) was obtained with four independent bottom electrical contacts and one common top electrical contact to actuate the microbeams separately or together. The electroactivity, actuation, blocking force and sensing of the proof-of-concept prototypes were characterized based on the microcomb configuration to evaluate the process suitability for PEDOT:PSS-based MTs.

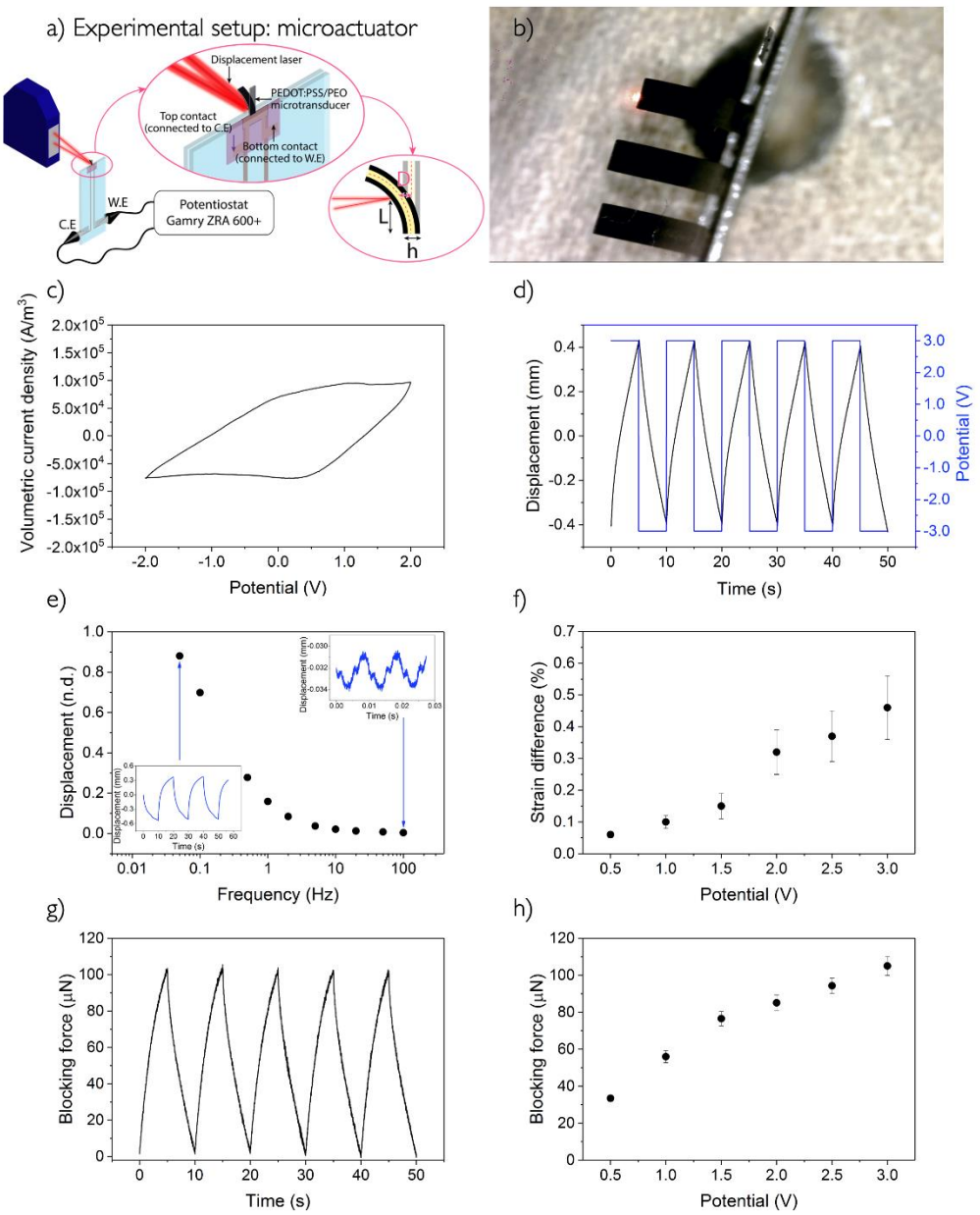

Figure 2. Electromechanical characterizations of a 2900 x 250 x 23 µm microbeams: (a) displacement measurement set-up (b) illustration of microbeam displacement, (c) cyclic voltammogram at a scan rate of 20 mV.s^{-1} in a voltage window of ± 2.0 V, (d) displacement and an applied potential as a function of time at a frequency of 0.1 Hz, (e) displacement vs. frequency and in inset displacement vs. time for two frequencies at an applied potential of ± 1.25 V, (f) strain difference as a function of applied potential at a frequency of 0.1 Hz, (g) blocking force as a function of time at an applied potential of ± 3.0V and a frequency of 0.1 Hz, (h) blocking force as a function of applied potential at a frequency of 0.1 Hz.

The characterized microbeam (2900 x 250 x 23 µm) is presented in figure 1(i). The thickness of the MTs (23 µm ± 2 µm) was measured using profilometry. In order to operate the resulting MTs in open-air, the ions necessary to the redox process of the ECP-based electrodes have to be incorporated as a last step. The MTs were then immersed for 72 h in neat ionic liquid, 1-ethyl-3-methylimidazolium bis(trifluoromethanesulfonyl)imide (EMImTFSI), allowing incorporation of this last element for obtaining electrochemical MTs. The displacement measurement set-up is based on laser triangulation as described in the figure (2a) and an image of three integrated actuator beams under an applied voltage is presented in the figure (2b) (video in supplementary materials). The electroactivity of the MTs was evaluated using cyclic voltammetry (figure 2(c)) in 2-electrode configuration and by calculating the volumetric charge density in order to evaluate the amount of electric charge per volume of the PEDOT:PSS electrodes.

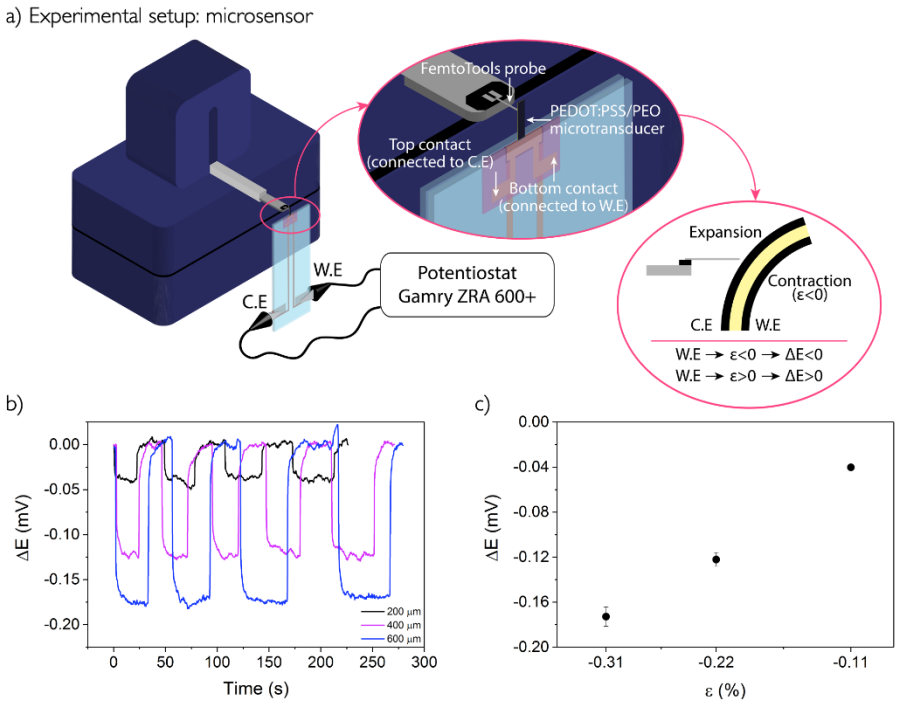

Figure 3. Sensor characterizations of a 2900 x 250 x 23 µm microbeams: (a) schematic representation of the experiment setup, (b) output voltage response to a mechanical stimulation of 200, 400 and 600 µm, (c) OCV response as a function of applied strain.

The PEDOT:PSS-based MT presents slightly defined oxidation and reduction peaks, indicating that a redox process is occurring. However, the MT presents asymmetry in the cyclic voltammogram compared to usual behavior of ECP trilayers with identical electrodes, pointing to different properties of the bottom and top PEDOT:PSS electrodes. This might be due to the reason that the top electrode is well protected throughout the process between Si wafer and ionically conducting membrane and is only exposed to XeF_2 vapor phase etching during the release step. In contrast, the bottom electrode can be damaged during IBE and photoresist processing steps, and consequently results in slightly weakened bottom electrode properties. Despite that, the calculated volumetric charge density of this PEDOT:PSS-based MT is 1.2 x 10^7 C m^{-3}, which is in the same order of magnitude as commonly reported values for ECPs.[26] Electrical stimulation of trilayer MTs is performed by ± 3V square wave potential at 0.1 Hz, leads to opposite volume variations of the electroactive electrodes and consequently to bending deformation of microactuator beams (figure 2(d)). The bending direction is occurring toward the anode, corresponding to a volume contraction during oxidation which is consistent with cation exchange mechanism, as already described for EMImTFSI electrolyte.[25] Figure 2(e) shows the displacement obtained as a function of frequency. As expected for electrochemical devices limited by ion diffusion speed, the amplitude of deformation is decreasing significantly when the frequency of electrical stimulation is increasing, but electromechanical response can still be observed at a frequency as high as 100 Hz thanks to the low thickness of these MTs. Since the absolute displacement depends on geometrical parameters, making a comparison difficult with other works, the corresponding strain difference was calculated according to Sugino *et al.*[27] for different applied potentials at 0.1 Hz and the results are presented in figure 2(f). It can be seen that the applied potential has an effect on the strain difference of the PEDOT:PSS-based microbeams, presenting common behavior of ECP based devices.[28–31] The microbeam presents relatively smooth increase in the strain difference, reaching the maximum value of 0.46 % at an applied potential of 3.0 V (video in Supplementary material). While increasing further the stimulation potential could slightly increase the maximum strain difference value, then these experiments were not conducted due to the risk of over oxidation and possible bad stability of the device. As another important parameter, the blocking force of the microbeams was evaluated. The applied potential tends to bend the microbeam and therefore to increase the forces (figure 2(f)). Measurements were carried out as a function of applied potential at a frequency of 0.1 Hz (figure 2(g)). It can be seen that, as for strain difference, the microbeam presents increasing trend in blocking force when the applied potential is increased and the maximum output force of the microbeam is 105 µN at 3.0 V. All the above characterized parameters

present classical behavior of non-integrated ECP-based actuators, indicating the relevance of the designed process. [25,28–32]

ECP based devices are also known to act as mechanical strain sensors, i.e. providing electrical energy output while mechanically stimulated. This feature is described widely for centimeter scale devices[26,33,34] and more recently on micrometer scale actuators.[25] However, since the microdevices described in this work are the first fully integrated MTs, their mechanical strain sensing has to be demonstrated. The microbeam (2900 x 300 x 23 µm) was mechanically stimulated by applying step displacements and the corresponding open circuit voltage (OCV) responses (ΔE) were recorded as a function of time (figure 3(a)). Figure 3(b) demonstrates the OCV response as a function of time to the mechanical step stimulation (200, 400 and 600 µm) of the PEDOT:PSS-based integrated microbeam. This response presents the same behavior with the ECP-based micrometer scale actuators.[25] The sign of the output voltage is negative when applied displacement leads to the compression of the working electrode. Based on the piezoionic mechanism, involving stress induced motion of the ions and their relative mobility, the expulsion of the more mobile EMI^+ cations from the mechanically compressed working electrode leads to the generation of negative open circuit potential.[25,35,36] Figure 3(c) demonstrates the increase in OCV response as a function of applied strain (step displacement of 200, 400 and 600 µm, corresponding to -0.11, -0.22 and -0.31 % strain difference). The maximum value of -0.17 mV is measured with an applied strain of -0.31 %. These results demonstrate for the first time that PEDOT:PSS-based MTs fully integrated in flexible chips are capable of detecting and quantifying mechanical stimulation and to produce an output voltage signal almost equivalent to non-integrated ECP-based microsensors (~0.2 mV at an applied strain of 0.3 %).[25]

3. Conclusions

This work demonstrated a successful microfabrication process to integrate very small air operating PEDOT:PSS-based microtransducers into foldable chips. The integrated gold connections, are in contact with the top and bottom PEDOT:PSS electrodes, which is indispensable in order to control MTs individually inside microdevices. The process combined different microfabrication technologies allowing batch fabrication of the microdevices on Si substrate without any manual handling during the process. This work demonstrated the full integration of freestanding MT microbeams, which is one of the expected milestones since 2000s. Furthermore, depending on the photomask design, more complex devices with bridges, membranes, etc. can be designed. Microbeam transduction was successfully evaluated by strain difference (0.46 %) and blocking force (105 µN), demonstrating the best performances of ECP based devices at this scale. Moreover, sensing property was evidenced for the first time on such small MTs, resulting in a maximum output voltage of -0.17 mV at an applied mechanical strain of -0.31 %. These results demonstrate that these proof-of-concept microbeams present common behavior of non-integrated ECP based devices and therefore, the microfabrication process does not damage extensively the resulting ECP-based microbeams. These chips can be easily hybridized with other flexible or non-flexible microsystems. The ECP-based MEMS described in this work not only solve the limitations of incompatible stiff MEMS with soft electronics but also the limitations of previously reported polymer-based microactuators such as limited integration level, low extend of deformation or use of high electric fields. PEDOT:PSS based-actuators could open new application fields for instance in medical devices that are in contact with soft human tissues, where discrete flexible devices integrated circuits and power sources are required.[37] Therefore, manufacturing with microfabrication technologies, polymeric materials with multiple functionalities as actuation and sensing are scientific and technological key elements for fabricating flexible microrobotic systems. The remaining challenges of such devices would concern their response speed, limited by ion diffusion, their cycling stability and their positioning control to perform precision tasks. This last goal will be study in link with the previous modeling works. [40,41]

4. Experimental Section

4.1 Materials

Poly(ethylene glycol) methyl ether methacrylate (PEGM, Mn = 500 g mol^{-1}), poly(ethylene glycol) dimethacrylate (PEGDM, Mn = 750 g mol^{-1}), ammonium persulfate (APS, 98 %), and cyclohexanone (>99.8 %) were obtained from Sigma Aldrich and used as received. Aqueous PEDOT:PSS dispersion (Clevios PH1000, solid content 1.0 – 1.3 wt%) was purchased from Heraeus Precious Metals GmbH & Co. Nitrile-butadiene rubber (NBR), initiator dicyclohexyl peroxydicarbonate (DCPD), and 1-ethyl-3-methylimidazolium bis(trifluoromethanesulfonyl)imide (EMImTFSI 99.9%) were used as supplied from LANXESS, Groupe Arnaud, and Solvionic, respectively. S1828 photoresist, SU-8 2000 series photoresists with different viscosities (2002, 2010, 2035, 2075), developer MF-319, and SU-8 developer were obtained from Microchem and used as provided and recommended by the manufacturer.

4.2 Microfabrication process:

As a first step, the alignment marks were fabricated on the backside of the 2-inch double-side polished Si wafer (150 µm) using a standard lift-off process of a positive photoresist S1828. Ti (20 nm) and Au (300 nm) were deposited on the patterned photoresist by evaporation and the lift-off was performed in acetone to create the designed Au patterns on the

Si wafer. The top electrical contacts were fabricated in the same way on the front side of the wafer, using different kind of photomask to create the patterns with desired shapes (figure 1(b)). In the third step of the process, a ring-shaped (60 µm) mold of negative photoresist SU-8 was prepared in order to cast the PEDOT:PSS solution and to fabricate trilayer actuator. The provided indications of the manufacturer were scrupulously followed for all the SU-8 layer steps. Next, the trilayer was fabricated using layer stacking method, comprised of two electroactive PEDOT:PSS electrodes sandwiching an ion storage membrane with semi-interpenetrating polymer network (semi-IPN) architecture as described elsewhere.[25] Thereafter, an Au layer (300 nm) was evaporated on top of the trilayer actuator and an SU-8 layer was spin-coated, exposed, and developed, resulting in 24 µm patterns. The next step involves etching of the exposed Au layer around the SU-8 patterns using IBE to create hard mask (Au and SU-8) for trilayer etching step. The argon ion beam operates at a gas pressure of $5x10^{-4}$ mbar where an ion current density of 300 µA cm^{-2} is obtained at an ion beam voltage of 700 V and a microwave power of 300 W. A 15 sccm ion beam sputter and an 8 sccm plasma bridge neutralizer flow rates were used. The etch rate of the gold is 15 $nm.min^{-1}$, i.e. the etching was finalized after 20 min, which was detected using secondary ion mass spectroscopy. Thereafter, RIE of polymer actuator was carried out in a gas mixture of O_2/CF_4 (90/10) with a power of 300 W and a pressure of 200 mTorr during 35 min (~ 0.65 µm min^{-1}).[23,38,39] The gold layer is known to be insensitive to oxygen-rich plasma etching, whereas the SU-8 photoresist mask is highly sensitive to the O_2/CF_4 gas mixture. The thickness of the SU-8 layer (24 µm) was chosen to be completely etched (2 µm min^{-1}) during the RIE of the trilayer actuator. Relatively thick SU-8 patterns were chosen in order to obtain high aspect ratio during etching, which helps to prevent under-etching, to obtain vertical walls of the MTs and consequently to decrease the risk of electrical damage of the MTs. After this step, MTs with desired shapes were obtained, also revealing the top Au electrical connections. In order to continue the process, the Au top electrodes were protected to be able to remove the Au layer from the surface of the MTs. Therefore, a 10 µm layer SU-8 was used to create the protections for revealed electrical contacts. Subsequently, Au etching was carried out using IBE in the same way as described previously to remove the layer from the surface of the microbeams. To avoid short circuits between the top and the bottom PEDOT:PSS electrodes during following steps in the process, an insulating SU-8 layer (2 µm) was formed to cover the edge of the MTs, where the bottom Au electrical contact will be created (figure 1(c)). Then, a 300 nm Au layer was evaporated over the entire structure to create the surface for the bottom electrical contacts. SU-8 photoresist was used to create the local patterns for the bottom electrical contacts directly on the Au layer in the same way as the protections for the top electrical contacts. IBE was used to remove the unprotected Au layer and to form SU-8 covered bottom electrical connections (figure 1(d)). Thereupon, the electrical contacts and part of the trilayer MTs were encapsulated in a 60 µm SU-8 layer to facilitate the manipulation of each chip (figure 1(e)). The stiffness of the final chip can be adjusted by tuning the thickness of this encapsulation layer. Finally, all the chips were released by etching thoroughly the Si wafer using vapor phase XeF_2 bulk isotropic etching (chamber 1.0 Torr, etching gas XeF_2 4.0 Torr, 600 cycles with a speed of 20 s/cycles). Both electrical contacts are accessible from one side of the flexible SU-8 encapsulation.

Experimental set up: The microdevices were placed between two glass plates covered with copper lines to connect them to the measurement system. The experiments were monitored from top and side using two Dino Lite AM7000/AD7000 micro cameras. During the actuation and blocking force measurements, the chips were connected to the voltage source (NF Electronic Instruments 1930) and an in-house amplifier to apply a square wave potential (0.5 – 3.0 V). The actuation displacement D was recorded with a laser LKG 32 Keyence displacement sensor and the strain difference ε was calculated by $\varepsilon=2Dh/(L^2+D^2)$[27] where *h* is the thickness of the actuator and *L* is the distance between the clamped end of the actuator and the measurement point on the beam. The blocking force of the microactuators was determined with a microforce sensing probe FT-S1000 (Femtotools) combined with a high-precision three-axis nanomanipulation unit (FT-RS1002 Femtotools). Cyclic voltammetry was performed with a Gamry Potentiostat/Galvanostat ZRA 600+ to evaluate the electroactivity of the transducers and the sensing was measured with an open circuit voltage option.

Acknowledgements

This project received funding from the European Union's Horizon 2020 research and innovation program under Marie Skłodowska-Curie grant agreement N° 641822 – MICACT and N° 857263 Twinnims. This work was partly supported by the French Government through the program PIA EQUIPEX LEAF (ANR-11-EQPX-0025), RENATECH MicroTIP (ANR-15-CE08-0032-0) and ROBOCOP (ANR-19-CE19-0026) projects.

References

[1] R. H. Baughman, *Synth. Met.* 1996, **78**, 339.
[2] E. Smela, O. Inganäs, Q. Pei, I. Lundström, *Adv. Mater.* 1993, **5**, 630.
[3] E. Smela, O. Inganäs, I. Lundström, *Science* 1995, **268**, 1735.
[4] E. Smela, M. Kallenbach, J. Holdenried, *J. Microelectromechanical Syst.* 1999, **8**, 373.
[5] E. W. H. Jager, E. Smela, O. Inganäs, *Sensors Actuators, B Chem.* 1999, **56**, 73.

[6] E. W. H. Jager, O. Inganäs, I. Lundström, *Science* 2000, **288**, 2335.
[7] E. W. H. Jager, E. Smela, O. Inganäs, *Science* 2000, **290**, 1540.
[8] P. F. Pettersson, E. W. H. Jager, O. Inganas, 1st Annu. Int. IEEE-EMBS Spec. Top. Conf. Microtechnologies Med. Biol. Proc. (Cat. No.00EX451) 2000, **56**, 1999.
[9] E. W. H. Jager, C. Immerstrand, K. H. Peterson, K. E. Magnusson, I. Lundström, O. Inganäs, *Biomed. Microdevices* 2002, **4**, 177.
[10] C. Immerstrand, E. W. H. Jager, K. E. Magnusson, T. Sundqvist, I. Lundström, O. Inganas, K. H. Peterson, *Med. Biol. Eng. Comput.* 2003, **41**, 357.
[11] E. Smela, *Adv. Mater.* 2003, **15**, 481.
[12] G. Alici, M. J. Higgins, *Smart Mater. Struct.* 2009, **18**, 065013.
[13] B. Gaihre, G. Alici, G. M. Spinks, J. M. Cairney, *Sensors Actuators, A Phys.* 2010, **165**, 321.
[14] B. Gaihre, G. Alici, G. M. Spinks, J. M. Cairney, *Sensors Actuators, B Chem.* 2011, **155**, 810.
[15] T. N. Nguyen, K. Rohtlaid, C. Plesse, G. T. M. Nguyen, C. Soyer, S. Grondel, E. Cattan, J. D. W. Madden, F. Vidal, *Electrochim. Acta* 2018, **265**, 670.
[16] Y. Zhong, S. Lundemo, E. W. H. Jager, *Smart Mater. Struct.* 2018, **27**, 1.
[17] A. Khaldi, C. Plesse, C. Soyer, E. Cattan, F. Vidal, C. Chevrot, D. Teyssié, *Proc. ASME 2011 Int. Mech. Eng. Congr. Expo.* 2011, **1**, 1.
[18] A. Khaldi, C. Plesse, C. Soyer, E. Cattan, F. Vidal, C. Legrand, D. Teyssié, *Appl. Phys. Lett.* 2011, **98**, 164101.
[19] E. W. H. Jager, N. Masurkar, N. F. Nworah, B. Gaihre, G. Alici, G. M. Spinks, *Sensors Actuators, B Chem.* 2013, **183**, 283.
[20] A. Maziz, C. Plesse, C. Soyer, C. Chevrot, D. Teyssié, E. Cattan, F. Vidal, *Adv. Funct. Mater.* 2014, **24**, 4851.
[21] A. Khaldi, A. Maziz, G. Alici, G. M. Spinks, E. W. H. Jager, *SPIE Smart Struct. Mater. Nondestruct. Eval. Heal. Monit.* 2015, **9430**, 94301R.
[22] A. Khaldi, A. Maziz, G. Alici, G. M. Spinks, E. W. H. Jager, *Sensors Actuators, B Chem.* 2016, **230**, 818.
[23] A. Maziz, C. Plesse, C. Soyer, E. Cattan, F. Vidal, *ACS Appl. Mater. Interfaces* 2016, **8**, 1559.
[24] A. Khaldi, D. Falk, K. Bengtsson, A. Maziz, D. Filippini, N. D. Robinson, E. W. H. Jager, *ACS Appl. Mater. Interfaces* 2018, **10**, 14978.
[25] K. Rohtlaid, G. T. M. Nguyen, C. Soyer, E. Cattan, F. Vidal, C. Plesse, *Adv. Electron. Mater.* 2019, **5**, 1.
[26] Y. Wu, G. Alici, J. D. W. Madden, G. M. Spinks, G. G. Wallace, *Adv. Funct. Mater.* 2007, **17**, 3216.
[27] T. Sugino, K. Kiyohara, I. Takeuchi, K. Mukai, K. Asaka, *Sensors Actuators, B Chem.* 2009, **141**, 179.
[28] J. D. W. Madden, P. G. A. Madden, I. W. Hunter, Smart Struct. Mater. 2001 Electroact. Polym. Actuators Devices 2001, 4329, 72.
[29] G. M. Spinks, G. G. Wallace, L. Liu, D. Zhou, *Macromol. Symp.* 2003, **192**, 161.
[30] R. Temmer, I. Must, F. Kaasik, A. Aabloo, T. Tamm, *Sensors Actuators B Chem.* 2012, **166–167**, 411.
[31] T. F. Otero, J. M. Sansinena, J. M. Sansiñena, *Bioelectrochemistry Bioenerg.* 1995, **38**, 411.
[32] N. Festin, A. Maziz, C. Plesse, D. Teyssié, C. Chevrot, F. Vidal, *Smart Mater. Struct.* 2013, **22**, 104005.
[33] T. Shoa, J. D. W. Madden, T. Mirfakhrai, G. Alici, G. M. Spinks, G. G. Wallace, *Sensors Actuators, A Phys.* 2010, **161**, 127.
[34] N. Festin, C. Plesse, P. Pirim, C. Chevrot, F. Vidal, *Sensors Actuators, B Chem.* 2014, **193**, 82.
[35] V. Woehling, G. T. M. Nguyen, C. Plesse, Y. Petel, Y. Dobashi, J. D. W. Madden, C. A. Michal, F. Vidal, *Multifunct. Mater.* 2019, **2**, 045002.
[36] M. S. Sarwar, Y. Dobashi, E. F. Scabeni Glitz, M. Farajollahi, S. Mirabbasi, S. Naficy, G. M. Spinks, J. D. W. Madden, *SPIE Smart Struct. Mater. Nondestruct. Eval. Heal. Monit.* 2015, **9430**, 943026.
[37] D. Y. Khang, J. A. Rogers, H. H. Lee, *Adv. Funct. Mater.* 2009, **19**, 1526.
[38] A. Khaldi, C. Plesse, C. Soyer, E. Cattan, F. Vidal, C. Legrand, D. Teyssié, *Appl. Phys. Lett.* 2011, **98**, 164101.
[39] A. Khaldi, A. Maziz, C. Plesse, C. Soyer, F. Vidal, E. Cattan, *Sensors Actuators, B Chem.* 2016, **229**, 635.
[40] M. Bentefrit, S. Grondel, C. Soyer, C., A. Fannir, E. Cattan, J. D. Madden, T. M. G. Nguyen, C. Plesse, F Vidal. *Smart Mater. Struct.* 2017, **26**, 9.
[41] N. T. Nguyen, Y. Dobashi, C. Soyer, C. Plesse, G. T. Nguyen, F. Vidal, E. Cattan, S. Grondel, J. D. Madden *Smart Mater. Struct.* 2018, **27**, 11.